ACS APPLIED MATERIALS & INTERFACES

Research Article

www.acsami.org

Highly Efficient Semitransparent Polymer Solar Cells with Color Rendering Index Approaching 100 Using One-Dimensional Photonic Crystal

Wenjuan Yu,[†] Xu Jia,[†] Yongbing Long,[‡] Liang Shen,*[,†] Yan Liu,[§] Wenbin Guo,[†] and Shengping Ruan[†]

[†]State Key Laboratory on Integrated Optoelectronics, College of Electronic Science and Engineering, Jilin University, 2699 Qianjin Street, Changchun 130012, People's Republic of China

[‡]School of Applied Physics and Materials, Institute of Thin Film and Nanomaterials, WuYi University, No. 22 Dongchen Cun, Jiangmen 529020, People's Republic of China

[§]Key Laboratory of Bionic Engineering (Ministry of Education), Jilin University, Changchun 130022, People's Republic of China

Supporting Information

ABSTRACT: Window application is the important aim for semitransparent solar cells (STPSC) investigation. Here, we demonstrate a method to achieve significantly improved color rendering index (CRI), depressed chromaticity difference (DC), and enhanced power conversion efficiency (PCE) simultaneously by introducing the one-dimensional photonic crystals (1DPCs) Bragg reflector structure onto the STPSC. The device performance is studied from aspects of color perception, electrical properties, and theoretical optical simulations. The STPSCs exhibit achromatic transparency nature color perceptions, especially for the STPSCs with 1DPCs (pairs $\geq$ 3) under AM 1.5G illumination light source, standard illuminant D65, and standard illuminant A. The excellent CRI is approaching 97 with lower DC about 0.0013 for the device with 5 pairs of 1DPC illumined by AM 1.5G illumination light source. At the same time, the PCE of STPSC devices with 5 pairs of 1DPC was improved from 4.87 $\pm$ 0.14% to 5.31 $\pm$ 0.13% compared to without. This method provides a facilitative approach to realizing excellent SPTSC window application.

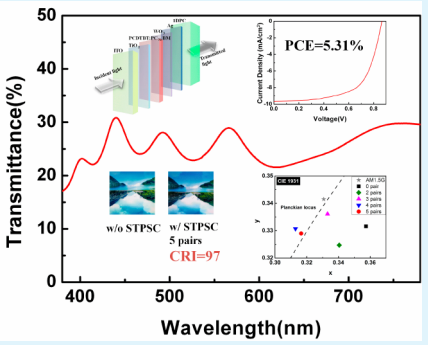

KEYWORDS: *STPSC, IDPCs, CRI, DC, CIE*

1. INTRODUCTION

Building integrated photovoltaic (BIPV) is a novel application of solar energy, which has been considered as an attractive area of research based on the combination of large area buildings and a huge photovoltaic market.[1−3] The BIPV not only requires supplying power but also needs aesthetics, natural lighting, and environment protecting.[4−7] So far, in order to relieve the application requirements, various photovoltaic architectures have been developed. Compared to the vacuum-deposited small molecule semitransparent organic solar cells[8] or silicon-based semitransparent solar cells,[9] semitransparent polymer solar cells (STPSCs) are identified as the most fitting role for BIPV applications[10−13] due to desirable features of flexibility, lightweight, and easy fabrication process.[14−16] In recent years, many promising improvements have been studied in the two contradictory characteristics, that is, power conversion efficiency (PCE) and transparency.[17,18] However, the current PCE of STPSCs is still lower than the normal PSCs due to the transmittance requirement, which hinders further applications toward integrating building.[19−21]

Considering the aesthetics and natural lighting of device design for building application, the natural quality of the light which penetrates STPSC is important. In 2010, the color characterization of STPSCs in an inverted structure has been studied first.[22] To satisfy the natural lighting purposes, it requires that the color rendering index (CRI) must approach 100 and the chromaticity color coordinates must be close to the Planckian locus at the same time.[23] Recently, in order to achieve a high PCE and transmittance with a natural light transmission, some research focusing on the CRI of STPSC has been reported, such as tandem structure with complementary absorbers (CRI = 97.2),[24,25] the incorporation with dyes (CRI = 98),[26] and a new low bandgap absorber with wide absorption (CRI = 86).[27] Although these devices have obvious enhancements in CRI performance, the drawbacks are also inevitable. For example, the STPSCs with low bandgap polymer PBDTTT-C-T have a high CRI because the absorption spectrum is broad and uniform alomost in the visible spectrum.[4] However, the perfect character is unique, and the synthesis process is relatively complex. Most of the other polymers do not have such a wide absorption spectrum. With doping of dyes in an active layer polymer as complementary absorbtion materials, a color neutral transparency perception was also achieved. However, the PCE fell by half owing to the

Received: March 8, 2015
Accepted: April 9, 2015
Published: April 9, 2015

DOI: 10.1021/acsami.5b02039
ACS Appl. Mater. Interfaces 2015, 7, 9920−9928

light loss in the dye and damage of the PEDOT:PSS electrode by mixing the dye. The tandem structure STPSCs with complementary absorption range is another promising strategy for high CRI. But the fabrication process is complicated. At the same time, though the CRI of these reported works are improved, the chromaticity difference (DC) is still higher than the tolerance of CRI calculation. If the DC is larger than 0.0054, the calculated CRI will become less accurate based on the CRI definition.[28−30] Consequently, how to achieve a high CRI close to 100 combined with DC lower than 0.0054 is a key problem for the STPSCs. It is necessary to design excellent device architectures to achieve an excellent natural color perception and a high PCE simultaneously.

In this work, we demonstrate a method to simultaneously achieve a high CRI of 97, a lower DC of 0.0013, and a higher PCE of 5.31%. The one-dimensional photonic crystals (1DPCs) Bragg reflector was introduced onto the transparent Ag top electrode of PCDTBT:$PC_{70}BM$ [poly[*N*-9″-heptadecanyl-2,7-carbazole-*alt*-5,5-(4′,7′-di-2-thienyl-2′,1′,3′-benzothiadiazole):[6,6]-phenyl C71-butyric acid methyl ester] based STPSC (Figure 1a), in order to balance the total device transmittance spectrum and enhance the color rendering properties. The 1DPC is composed of alternated layers of MoO_3 and LiF. The extinction coefficients of the two materials are both lower than 0.001 in the visible range which means they nearly do not absorb the light. Then, they can be evaporated easily to form uniform films in the 1DPC fabrication process. PCDTBT has a deeper highest occupied molecular orbital (HOMO) energy level which was reported in 2007.[31−33] The absorption range of PCDTBT:$PC_{70}BM$ is mainly located in wavelength (λ) < 600 mn, which is relatively narrow compared to the whole visible region (380−780 nm). Therefore, the color perception and CRI of PCDTBT-based STPSCs cannot meet the requirements of the applications. Fortunately, the special optical properties of 1DPC can remedy the absorption limitation of PCDTBT. In previous study,[34−36] 1DPC always was designed to reflect light within the absorption range of the active layer while maintaining a fine transmittance in complementary visible wavelength by utilizing its photonic bandgap characteristic. In order to obtain the largest PCE, the period of 1DPC is usually bigger than 6. In addition, the color perception is not mentioned. Here, we use the 1DPC Bragg reflector concept to design the lower period multilayer system. When the period is not big enough, the photonic bandgap cannot be formed completely, which can realize the weak transmittance selectivity in the photonic bandgap range. To take this factor into consideration, we designed the center of the photonic bandgap of 1DPC as 730 nm. The complementary transmittance spectrum of 1DPC and the light absorption range of PCDTBT led to a uniform flat transmittance spectrum of STPSC by optimizing the period of 1DPC. In other words, the 1DPC could level the concavo-convex transmittance spectrum induced by the absorption of PCDTBT. Since the light reflected by 1DPC is coming back into the device, the inside optical electric field ($|E(x)|^2$) will be re-distributed and influence the PCE. At the same time, the total transmittance also can be changed due to the incompletely formed photonic bandgap of 1DPC. By tuning the pairs of 1DPC, the PCE of STPSCs increases from 4.87 ± 0.14% to 5.31 ± 0.13% with the corresponding transmittance ranging from 28.4 ± 1.1% to 25.1 ± 1.1%. The increased PCE is caused by the optical electric field re-distribution. Although the transmittance decreased, it also meets the requirement of applications (≥25%).[4] It is worth noting that the CRI of STPSC is increased from 84 to 97 with 5 pairs of 1DPC under AM 1.5G illumination light source. The DC is 0.0013, that being much lower than 0.0054. It means that the STPSC with 1DPC exhibits extraordinary rendering capacities and color perceptions. This method can achieve excellent STPSCs with CRI approaching 100 and provide a new method for window application.

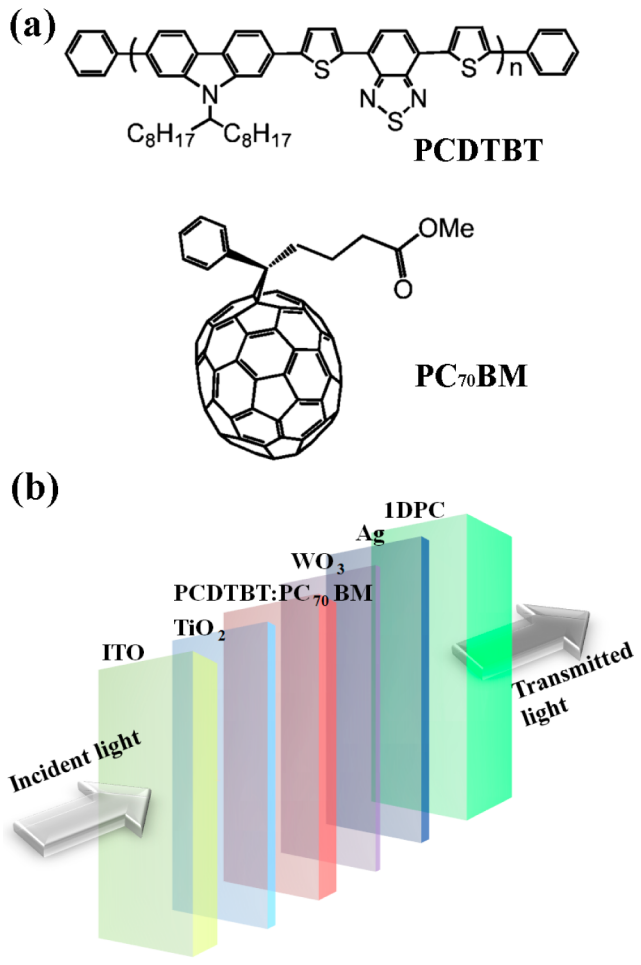

Figure 1. (a) Molecular structures of PCDTBT and $PC_{70}BM$. (b) Device architecture of STPSC with 5 pairs 1DPCs with incident light and transmitted light.

2. EXPERIMENTAL SECTION

The preparation of devices is described as followed and shown in Figure 1b. The control STPSC structure is glass/ITO(150 nm)/TiO_2(25 nm)/PCDTBT:$PC_{70}BM$ (80 nm)/WO_3(10 nm)/Ag(15 nm). The 1DPCs-based STPSCs structure is control STPSC/$[MoO_3/LiF]^{pairs}$. First, the ITO glass substrate was cleaned by acetone, ethanol, and deionized water for 30 min, respectively. Then, TiO_2 was prepared as the electron transport layer by sol−gel methods with controlled thickness. PCDTBT (Lumtec Corp.) and $PC_{70}BM$ (Lumtec) were dissolved in 1,2-dichlorobenzene to produce a 7 mg/mL solution within a 1:4 weight ratio and stirred for 2 days in a glovebox. The thin film of PCDTBT:$PC_{70}BM$ (80 nm) was prepared by spin coating at 2000 rpm for 30 s and annealing at 70 °C for 30 min in a glovebox. Then, the 10 nm WO_3 and 15 nm Ag were deposited in sequence under 5×10^{-4} Pa vacuum. In order to define the active area of the STPSC, the Ag top electrode was deposited through a shadow mask. The dimension of the STPSC was 0.064 cm^2. The deposition

DOI: 10.1021/acsami.5b02039
ACS Appl. Mater. Interfaces 2015, 7, 9920−9928

rate was monitored by a quartz-oscillating thickness monitor (ULVAC CRTM-9000), which is about 0.3 nm/s. For the STPSC with 1DPCs, the different pairs of MoO_3 (86.5 nm)/LiF (126.7 nm) were alternately evaporated under vacuum (5×10^{-4} Pa) and the rate of deposition was about 1 nm/s. The pairs of 1DPC are 2, 3, 4, and 5.

The absorption, transmittance, and reflectance spectra were measured by an ultraviolet/visible spectrometer (UV1700, Shimadzu). $J-V$ characteristics were measured by a Keithley 2601 source meter under Oriel 300 W solar simulator with the intensity of a 100 mW/cm^2 AM 1.5G illumination light source. The light source intensity was measured by a photometer (International Light, IL1400). The IPCE was measured by a Crowntech QTest Station 1000AD.

3. EXPERIMENTAL AND SIMULATION RESULTS AND DISSCUSSION

3.1. Device Color Perception. In order to explore the potential of STPSCs with 1DPC reflector for window application, we have fabricated several STPSC devices based on PCDTBT:$PC_{70}BM$ as active layer materials. As shown in Figure 1b, the device architecture is ITO/TiO_2/PCDTBT:$PC_{70}BM$/WO_3(10 nm)/Ag(15 nm)/1DPC ($[MoO_3/LiF]^{pairs}$). The 1DPC ($[MoO_3/LiF]^{pairs}$) reflector is composed of alternated deposit layers of MoO_3 and LiF.

First, to design an appropriate Bragg reflector, the transmittance and reflectance spectra of 2, 3, 4, and 5 pairs of 1DPCs and the absorption spectrum of PCDTBT:$PC_{70}BM$ are measured and shown in Figure 2a,b, respectively. As we know, 1DPCs are a multilayer reflector. The refractive index is periodic in one-dimensional that can create a photonic bandgap with a range of "forbidden" frequencies.[37−42] Here, we define the two period thickness, and refractive index is d_1, d_2, n_1, and n_2, respectively. There is a relationship between n_1, n_2, d_1, and d_2 for a quarter-wave stack, in which the optical path of each layer is one-quarter of the center wavelength (λ_0). The relationship formulation is listed as follows:

$$n_1 d_1 = n_2 d_2 = \frac{\lambda_0}{4} \quad (1)$$

According to formulation (1), we fabricate the 1DPC using high refractive index materials, MoO_3, and low refractive index materials, LiF, as the periodic unit components. As shown in Figure 2a, the transmittance of 1DPC over 600 nm is decreased with the increasing pairs. PCDTBT:$PC_{70}BM$ film mainly absorbs green-yellow light below 600 nm. Therefore, the STPSCs with PCDTBT:$PC_{70}BM$ always appear crimson color. In order to tune the color of STPSCs toward a natural color (no special color) to maintain the application requirement, we design the 1DPCs with complementary reflectance spectrum. Here, we set 730 nm as λ_0. The refractive indices of MoO_3 and LiF are 2.11 (n_1) and 1.44 (n_2), respectively. According to formulation (1), the thicknesses of MoO_3 and LiF can be calculated, which are 86.5 and 126.7 nm, respectively. It is obvious that the reflectance intensity in more than 600 nm is increased gradually with increasing pairs of 1DPC.

Figure 3 shows the total device transmittance spectra of respective STPSCs with different pairs of 1DPC. The spectrum of STPSC without 1DPC is also taken for comparison. With different pairs of 1DPC, the shapes of the spectra curves changed remarkably, showing the flexibility of transparency management through 1DPC reflector. For the control STPSC without 1DPC, the shape of the transmittance spectrum is concavo-convex due to the PCDTBT:$PC_{70}BM$ absorption. In order to balance the transmittance spectrum, the 1DPCs with opposite transmittance property are designed. The average visible transmittance (AVT) in the visible region (380−780 nm) is presented in Table 1. As the pairs of 1DPC vary from 0 to 5, the AVT can decrease from 28.4% to 25.1% caused by the reflectance of 1DPC, but it is still satisfied with the application requirement. In the wavelength range below 600 nm, there are several small vibrations, which correspond to the 1DPC transmittance spectra. The higher pairs of 1DPC are accompanied by the lower transmittance in the red region of the visible spectrum. In perceptual intuition, the tall tail of the transmittance curve is brought down with higher pairs of 1DPC. The amplitudes of the transmittance spectra are gradually decreased. Especially, the transmittance spectrum for a device with 4 or 5 pairs of 1DPC is almost oscillated

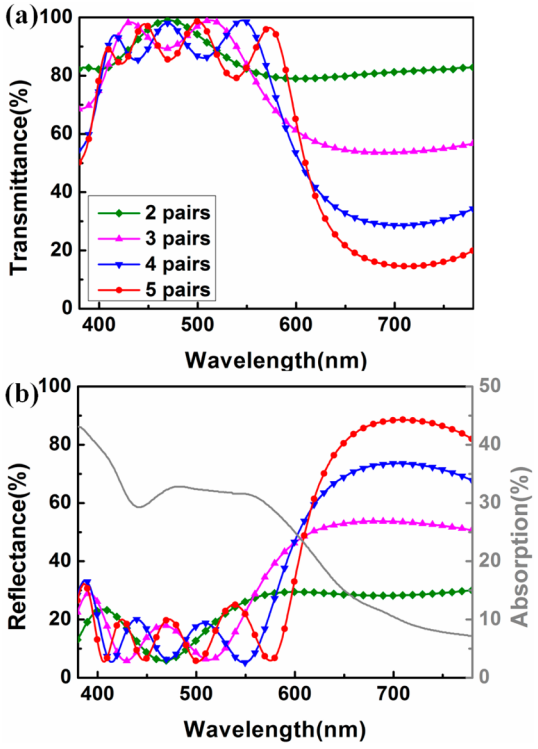

Figure 2. (a) Transmittance spectra of 1DPCs. (b) Reflectance spectra of 1DPCs corresponding to the left axis and the absorption spectrum of PCDTBT:$PC_{70}BM$ with gray line corresponding to the right axis.

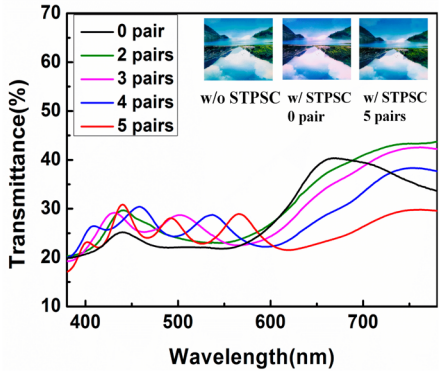

Figure 3. Total transmittance spectra of different devices with 0, 2, 3, 4, and 5 pairs of 1DPC. Inset: Photograph of computer display background without STPSC and with STPSC (0 pair and 5 pairs).

DOI: 10.1021/acsami.5b02039
ACS Appl. Mater. Interfaces 2015, 7, 9920−9928

Table 1. Detail Performance Parameter under 100 mW/cm^2 Simulated AM1.5G in Ambient Air and the AVT of 0, 2, 3, 4, and 5 Pairs of 1DPC Devices

devices	J_{sc} (mA/cm^2)	V_{oc} (V)	FF (%)	PCE (%)	AVT (%)
0 pair	8.86 ± 0.11	0.87 ± 0.01	63.2 ± 0.03	4.87 ± 0.14	28.4 ± 1.1
2 pairs	9.36 ± 0.10	0.87 ± 0.01	63.4 ± 0.02	5.16 ± 0.13	30.1 ± 1.3
3 pairs	9.52 ± 0.07	0.87 ± 0.01	63.3 ± 0.03	5.24 ± 0.13	29.4 ± 0.9
4 pairs	9.59 ± 0.09	0.87 ± 0.01	63.2 ± 0.03	5.27 ± 0.14	27.8 ± 1.0
5 pairs	9.67 ± 0.08	0.87 ± 0.01	63.1 ± 0.04	5.31 ± 0.13	25.1 ± 1.1

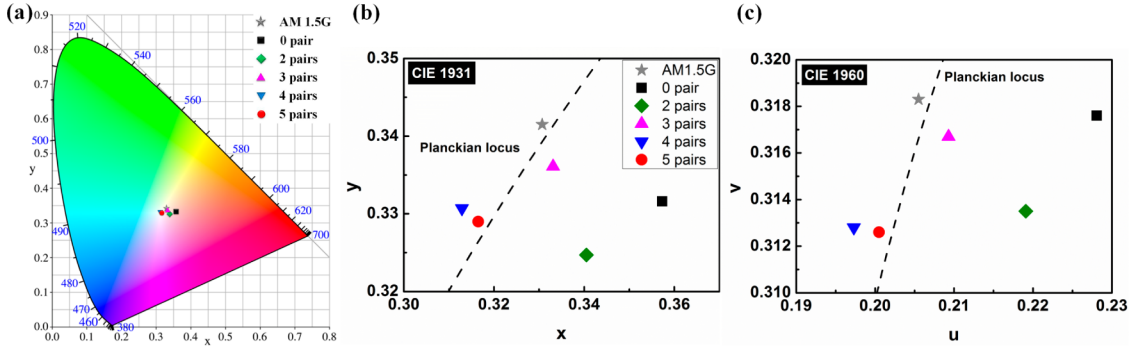

Figure 4. (a) Representation of the color coordinates of the STPSC devices with different pairs of 1DPC under AM 1.5G illumination light source on the CIE 1931 color space. Detailed section (b) of CIE 1931 color space and (c) of CIE 1960 uniform color space under AM 1.5G illumination light source.

infirmly over the entire visible spectrum. Such flat spectra mean the transmittance light remains the color perception of the original light source. The photographs of devices without 1DPC and with 5 pairs of 1DPC are inserted in Figure 3. To distinguish the color change of the incident light, the incident light is chosen from the computer display. It can be seen that the background color was only slightly dark through the STPSC. But for the device without 1DPC, the background color shifted to crimson. It is easy to understand that the incident light is almost white and the transmitted light is turned into gray by the STPSC. It is owing to the high CRI of the device with 5 pairs of 1DPC.

To analyze the device transparency color perception quantitatively, the color coordinates (x, y) on the CIE 1931 color space and (u, v) on the CIE 1960 uniform color space,[43] correlated color temperature (CCT), and DC from the transmittance spectra are calculated and illustrated as follows.[44] The color coordinates can imply how the light changed when it transmitted though STPSC. CCT is the color temperature of the nearest point on the Planckian locus. In the calculation of CRI, the corresponding reference illuminant is determined by CCT. When the corresponding reference illuminant is sure, the availability of CRI is confirmed by the DC.

The color coordinates (x, y) on the CIE 1931 color space and (u, v) on the CIE 1960 uniform color space are shown in Figure 4. Because the color perception and the CRI are strongly dependent on the incident light, three light sources have been chosen, including the AM 1.5G illumination light source, standard illuminant D65, and standard illuminant A. The transmitted light is represented by the product of the transmittance spectra of each STPSC with different pairs of 1DPC. The relative spectral power distribution of CIE standard illuminant A is the Planckian radiator at a temperature of about 2856 K. CIE standard illuminant D65 has a CCT of approximately 6500 K which is intended to represent average daylight.

Figure 4a displays the CIE 1931 color space and represents the color coordinates position of each device illuminated by the AM 1.5G illumination light source and also the color coordinates position of the AM 1.5G illumination light source. The color coordinates position of each device illuminated on the CIE 1931 color space by the standard illuminant D65 and standard illuminant A are shown in Supporting Information Figures S1a and S2a. The summarized color coordinates are shown in Supporting Information Table S1. The color coordinates of the AM 1.5G illumination light source are located in the white point (around (0.33, 0.33)). The color coordinates can imply how the light changed when it transmitted though STPSC. In other words, if the color coordinates varied obviously, it means that the incident light will be changed a lot after running through the STPSC. When the light of AM 1.5G illumination and standard illuminants D65 and A transmitted from the STPSC device without 1DPC (0 pair), the color of the transmitted light is changed and located in the low colorfulness area on the CIE 1931 color space [(0.3573, 0.3316), (0.3373, 0.3197), and (0.4817, 0.3895)]. The specific manipulated color coordinates are illustrated in Figure 4b, and Supporting Information Figures S1 and S2. Obviously, the incorporation of 1DPC with increasing pairs can shift the color coordinate to the Planckian with all three light sources.

Because of the nonuniform color of the CIE 1931 color space, the same distance on the CIE 1931 color space does not mean the same color change. So, in order to show the color change, the color coordinates (u, v) and the Planckian locus on the CIE 1960 uniform color space are also given in Figure 4c for the AM 1.5G illumination light source. The Planckian locus is known as the trace of the blackbody emission spectrum in a particular color space.[45] In Figure 4c, the color coordinates of devices with 0, 2, 3, 4, and 5 pairs of 1DPC are deviated from the Planckian locus, and the deviated distances are different from each other. For the device without 1DPC, the color coordinate is far away from the Planckian locus. But for the

DOI: 10.1021/acsami.5b02039
ACS Appl. Mater. Interfaces 2015, 7, 9920−9928

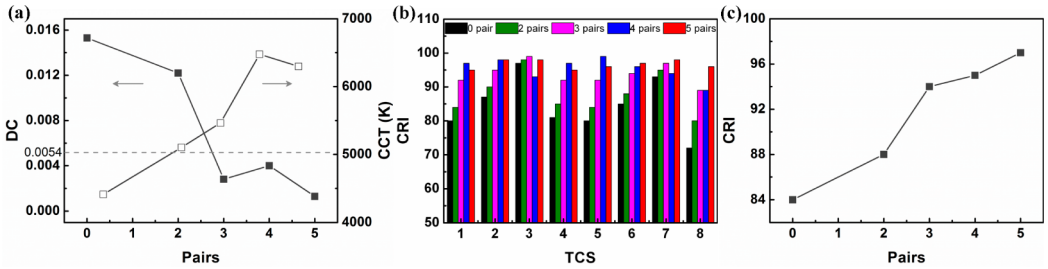

Figure 5. (a) DC and CCT of different pairs of 1DPC under illumination of AM 1.5G illumination light source. The dashed horizontal line marks DC = 0.0054. (b) CRI_i of TCS of different pairs of 1DPC under illumination of AM 1.5G illumination light source. (c) Average CRI of devices under illumination of AM 1.5G illumination light source.

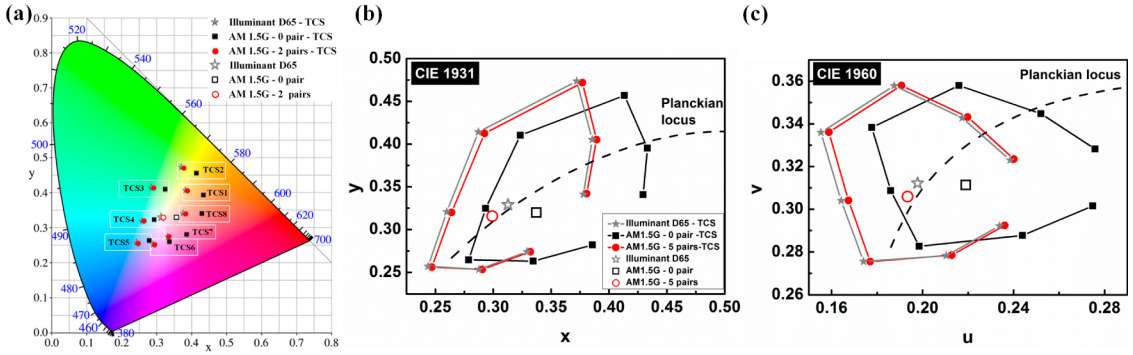

Figure 6. (a) TCSs color coordinates of devices with 0 pair and 5 pairs of 1DPC under AM 1.5G illumination light source and the TCSs color coordinates of reference standard illuminant D65 on the CIE 1931 color space. Detailed section (b) of CIE 1931 color space and (c) of CIE 1960 uniform color space under AM 1.5G illumination light source. Along with the anticlockwise start point of the TCS circle, the one by one point represents TCS1−TCS8.

device with 3, 4, and 5 pairs of 1DPC, the color coordinates are located close to the Planckian locus. For these color coordinates that are not exact on the Planckian locus, the CCT is defined and shown in Figure 5a. CCT is the color temperature of the nearest point on the Planckian locus, the color of which most closely resembles that of a given stimulus under specified viewing conditions and at the same brightness.[46] In the calculation of CRI, the corresponding reference illuminant is determined by CCT. Accordingly, we calculate CCT = 5575, 6500, and 2856 K for the AM 1.5G illumination light source and standard illuminants D65 and A (Supporting Information Table S1). When the light source is illuminated from the STPSC with different 1DPC, the CCT is changed. For a device without 1DPC, the CCT corresponds to 4411 K with the AM 1.5G illumination light source. For the device with 3 pairs of 1DPC, the CCT is about 5464 K, which is near to the AM 1.5G illumination light source. Compared to the three light sources, AM 1.5G illumination and standard illuminants D65 and A, the CCT variation of the device without 1DPC is larger than device with 1DPCs. It is clear that the color feature of light transmitted from the device without 1DPC is changed. However, by introducing 1DPC into the STPSC, the light property can be maintained. As we know, the CCT cannot exactly depict the color perception of STPSC. Therefore, the CRI is investigated forward.

Figure 5 shows the correlated parameters in CRI calculation. The CRI is an effective measurement of the ability for a light source. It can reveal the colors of various objects compared to an ideal or natural light source[47,48] which is defined by the Commission Internationale de L'Eclairage (CIE, in French). Here, the CRI accounts for the transmitted light color perception of STPSCs. STPSCs with a high CRI are desirable in window integration applications. To determinate the CRI of the transmitted light from the AM 1.5G illumination light source, standard illuminant D65 and standard illuminant A, the CIE 13.3-1995 standard procedure is followed.[25] Note that the CRI is considered to be meaningful only if the color coordinates lie within a chromaticity difference (DC) < 0.0054 from the Planckian locus on the CIE 1960 uniform color space as recommended by CIE. The DC of our devices illuminated by AM 1.5G illumination light source are shown in Figure 5a. When the corresponding reference illuminant is fixed, the availability of CRI is confirmed by the DC. The DC of the device without 1DPC is higher than 0.0054, but it is much lower when the pairs of 1DPC are more than 3. The variation of DC is obviously decreased from 0.0153 to 0.0013 with 5 pairs of 1DPC. With standard illuminants D65 and A, the DCs of devices are also decreased, which are shown in Supporting Information Figures S3 and S4.

The test sample method (TSM) is used to analyze the CRI perception. In the CIE (1995) definition, the original 14 test color samples (TCS) are taken from an early edition of the Munsell Atlas. The first eight TCSs are proposed in Nickerson (1960). They represent the relatively low saturated colors.[49] These eight TCSs are employed to calculate the general CRI. The last six TCSs provide supplementary information about the color rendering properties of the light source. Here, we just calculated the CRI by an average of the CRI_i of first eight TCSs (1−8). The CRI_i of 8 TCSs of different devices illuminated from the AM 1.5G illumination light source are shown in Figure 5b. The general CRI, which is the average of CRI_i, is depicted in Figure 5c. The CRI_i calculation method is illustrated as follows. First, the color coordinate on CIE 1931 and CIE 1960 color spaces, CCT, and DC (see earlier text) are

DOI: 10.1021/acsami.5b02039
ACS Appl. Mater. Interfaces 2015, 7, 9920−9928

calculated. Second, the color coordinates of the transmitted light with three light sources of the device without 1DPC and the device with 5 pairs of 1DPC reflected by each TCS are found. Then, according to the device CCT, different reference white light sources to illuminate the TCS presumptively are chosen. According to the CIE definition, in the case of CCT > 5000 K, the reference white light source is standard illuminant D; otherwise the a blackbody radiator is used for reference. Both reference white light sources should have the same CCT. Finally, by comparing the device TCS location and the reference TCS location, the CRI_i can be achieved.

In Figure 5b,c, the CRI has an enhancement by using 1DPC. According to the DC definition, the CRI of 3, 4, and 5 pairs of 1DPC devices are accurate. The CRIs of all of these devices are close to 100. Specially, the device with 5 pairs of 1DPC exhibits excellent CRI of 97 with lower DC of about 0.0013 under the AM 1.5G illumination light source. As far as we know, this accurate value is the highest CRI following with the lowest DC ever reported for the STPSC. The CRI_i of 8 TCSs of the different devices illuminated from standard illuminants D65 and A are shown in Supporting Information Figures S3 and S4. Considering the lower DC, the device with 3 pairs of 1DPC has the best DC (about 0.0005) under standard illuminant D65.

To understand the CRI calculation progress, the TCSs color coordinates on the CIE 1931 color space are illustrated in Figure 6a and Supporting Information Table S2. By observing the distance between the TCSs color coordinates of the device and its reference illuminant, we can easily obtain how the STPSC devices control the incident light. For example, if TCS4 is changed obviously, the corresponding color of incident light will be also changed distinctly. For the AM 1.5G illumination light source, the reference white light source with 5 pairs of 1DPC device is standard illuminant D65 according to the CIE definition. Because the reference white light source of the device without 1DPC is not the standard illuminant D65 with CCT lower than 5000 K, Figure 6 only gives the color coordinates of TCSs illuminated by reference standard illuminant D65 for comparison. We can visually determine the CRI by comparing the distance of the same TCS. To identify the distance clearly, the color coordinates (x, y) on the CIE 1931 color space and (u, v) on the CIE 1960 uniform color space are magnified, which are shown in Figure 6b,c. Along with the anticlockwise start point of the TCS circle, the one by one point represents TCS1−TCS8. The TCSs color coordinates on both the CIE 1931 color space and the CIE 1960 uniform color space of the device without 1DPC are far away from the TCSs illuminated by the reference source in both of the two color spaces, which indicates the poor CRI of about 84. As implied by the excellent CRI of 97, the color coordinates of TCSs illuminated by the transmitted light from the device with 5 pairs of 1DPC are close to the TCSs illuminated by the reference illuminant D65 both on the CIE 1931 color space and the CIE 1960 uniform color space, clearly demonstrating the superior color perception of this novel structure of STPSC. The TCSs color coordinates on the CIE 1931 color space and the CIE 1960 uniform color space with standard illuminants D65 and A are also illustrated and compared in Supporting Information Figures S5 and S6. Both of the TCS color coordinates of the devices with three light sources are listed in Supporting Information Table S2.

3.2. Device Electrical Properties. Figure 7 shows the $J-V$ and IPCE characteristics of the STPSC PCDTBT:$PC_{70}BM$ devices with different pairs of 1DPC. The $J-V$ characteristics

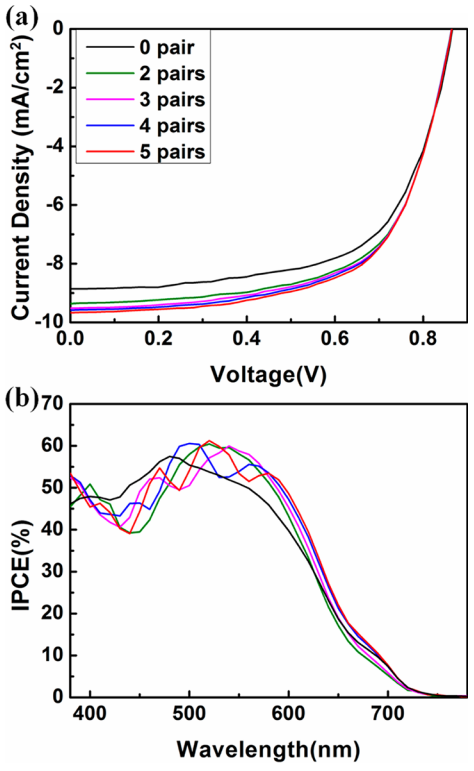

Figure 7. (a) $J-V$ characteristics of devices, under 100 mW/cm^2 simulated AM 1.5G illumination light source in ambient air. (b) IPCE characteristics of devices.

and relevant parameters of devices based on different pairs of 1DPC are shown in Figure 7a and Table 1. The device without 1DPC exhibits a PCE of 4.87 ± 0.14% with a circuit current density (J_{sc}) of 8.86 ± 0.11 mA/cm^2, an open-circuit voltage (V_{oc}) of 0.87 ± 0.01 V, and a fill factor (FF) of 63.2 ± 0.03%. The device with 5 pairs of 1DPC exhibits a higher PCE of 5.31 ± 0.13% with a J_{sc} of 9.67 ± 0.08 mA/cm^2, a V_{oc} of 0.87 ± 0.01 V, and a FF of 63.1 ± 0.04%. It is clearly observed that the V_{oc} and FF of the devices are almost the same, which can be attributed to FF and V_{oc} being independent of the 1DPC. Meanwhile, the J_{sc} is improved gradually with the increase of (MoO_3/LiF) pairs. We have demonstrated that the light lower than 600 nm is partly transmitted, but some light will be reflected back into the device for the second absorption. The decrease of total transmittance brings enhanced light absorption, which results in the increasing PCE.

The IPCE spectra tests for devices are shown in Figure 7b. Compared to the total transmittance of the devices, the IPCE shapes of different devices are in line with the 1DPC transmittance spectra. When the transmittance is higher, the IPCE is lower corresponding to the same wavelength. The IPCE spectrum of the device with 5 pairs of 1DPC has a little enhancment compared to the device without 1DPC. The improvement of IPCE is attributed to light reabsorption reflected by the 1DPCs. Hence, the improvement of device electrical performance is owing to the reflectance of 1DPC. It is clearly the STPSC device with 1DPC that achieves not only an excellent CRI and lower DC but also an increasing PCE.

3.3. Theoretical Optical Simulations. Here, the transfer matrix method (TMM)[50−52] is used to investigate the improvement resulting from the 1DPCs. The optical electric field distribution ($|E(x)|^2$), absorption spectra, and $J_{sc\,max}$ were

DOI: 10.1021/acsami.5b02039
ACS Appl. Mater. Interfaces 2015, 7, 9920−9928

calculated. In the simulation. All layers are assumed to be planar and isotropic, and the thickness of each layer is chosen by the experimental data.

To further prove the J_{sc} enhancement in STPSC with 5 pairs of 1DPC, the $(|E(x)|^2)$ in devices without 1DPC and with 5 pairs 1DPC are calculated and shown in Figure 8. Obviously,

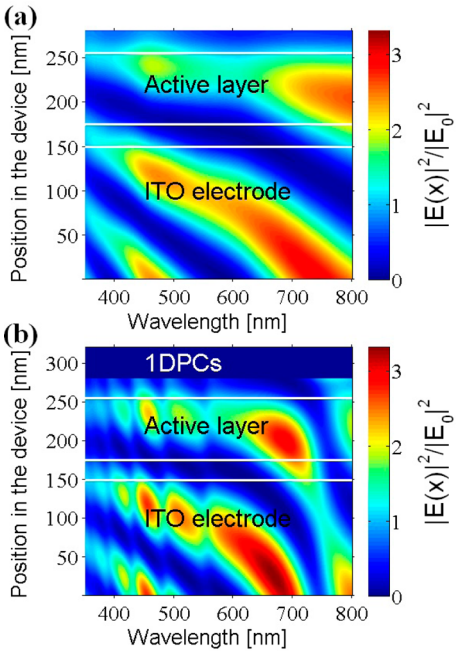

Figure 8. (a) Distribution of normalized modulus square of the optical electric field of device without 1DPC. (b) Distribution of normalized modulus square of the optical electric field of device with 5 pairs of 1DPC. $|E_0|^2$ is the modulus square of the optical electric field for the incident light.

the $(|E(x)|^2)$ in the active layer of the device with 5 pairs of 1DPC is higher than that without. This higher $(|E(x)|^2)$ is caused by the light reflected by 1DPCs that results in the higher J_{sc} and IPCE. The other $|E(x)|^2$ in the device with 2, 3, and 4 pairs of 1DPC are calculated and shown in Supporting Information Figure S7. They are also changed by reflection of the 1DPCs.

The changes of $(|E(x)|^2)$ in devices influence the optical absorption of the PCDTBT:$PC_{70}BM$ layer. So, in order to clarify the absorption enhancement, the absorption spectra of devices without 1DPC and with 2, 3, 4, and 5 pairs of 1DPCs are calculated and shown in Figure 9a in three-dimensional coordinate for feasible distinction. There is a dramatic difference of absorption spectra shapes for the devices. First, the shape of the absorption spectra is in line with the IPCE. Then, for the device with 5 pairs of 1DPC, the absorption is higher than that for the device without 1DPC in most visible wavelengths. The improvement originates from light reabsorption in the active layer caused by 1DPCs reflection.

Finally, the enhanced J_{sc} is also confirmed in simulation with the assumption that all absorbed photons are converted into charges and the devices are illuminated by the AM 1.5G illumination light source at 100 mW/cm^2. We named the upper limit to photocurrent generation as $J_{sc\,max}$.[53,54] The $J_{sc\,max}$ is calculated as a function of the pairs of 1DPC in Figure 9b. When the pair increased from 2 to 5, $J_{sc\,max}$ is gradually enhanced. With higher pairs, the $J_{sc\,max}$ is saturation. For devices without 1DPC and with 5 pairs of 1DPC, the $J_{sc\,max}$ are about 8.97 and 9.71 mA/cm^2. It indicates that the device with 5 pairs of 1DPC can achieve higher $J_{sc\,max}$. As is shown, the most excellent device is based on 5 pairs of 1DPC in optical and electrical properties. The theoretical optical simulations of devices indicates the 1DPCs play an important role in the device electrical properties and color perception.

4. CONCLUSION

In conclusion, we have successfully introduced the 1DPC structure onto the STPSC with significantly improved CRI, decreased DC, and enhanced PCE. We investigated the device performance from aspects of device color perception, device electrical properties, and theoretical optical simulations. The STPSC devices under the AM 1.5G illumination light source and standard illuminants D65 and A exhibit achromatic color perceptions, especially for the devices with 1DPC (pairs $\geq$ 3). The color coordinates of transmitted light are close to the Planckian locus. In TSM, the color coordinates of TCSs

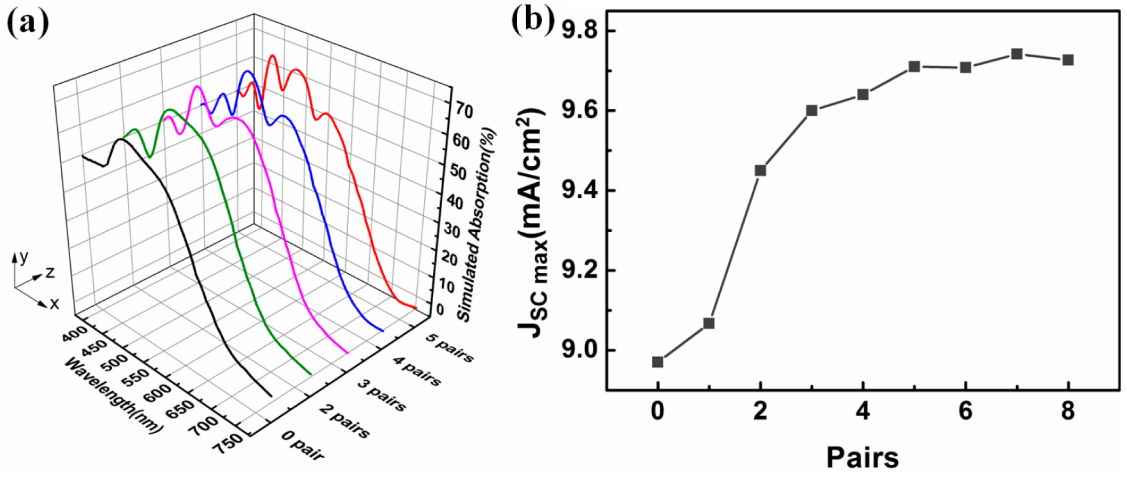

Figure 9. (a) Simulated absorption spectra of device without 1DPC and with 5 pairs of 1DPC. (b) $J_{sc\,max}$ as a function of the pair of 1DPCs and the improvement in $J_{sc\,max}$ as a function of the pair of 1DPCs.

DOI: 10.1021/acsami.5b02039
ACS Appl. Mater. Interfaces 2015, 7, 9920−9928

illuminated by the transmitted light of the device with 5 pairs of 1DPC is close to the TCSs illuminated by the reference source, clearly demonstrating the superior color perception of this novel structure of STPSC. The excellent CRI of 97 with lower DC of about 0.0013 under the AM 1.5G illumination light source and the lowest DC of about 0.0005 with CRI of 95 are achieved successfully, following with the increasing PCE of 5.31 ± 0.13%. This method reported here exhibits excellent color perception properties and enhanced electrical properties, which provides a facilitative approach toward realizing the SPTSC window application.

■ ASSOCIATED CONTENT

Supporting Information

Additional discussion of the analysis, color coordinates, DC, CRI, CRI_i, and TCSs, of the STPSC devices with different pairs of 1DPC under illuminants D65 and A, distribution of the normalized modulus square of the optical electric field of the device, and summarized data of different device pairs of 1DPC under AM 1.5G illumination light source, standard illuminant D65, and standard illuminant A. This material is available free of charge via the Internet at http://pubs.acs.org.

■ AUTHOR INFORMATION

Corresponding Author

*E-mail: shenliang@jlu.edu.cn.

Notes

The authors declare no competing financial interest.

■ ACKNOWLEDGMENTS

We are grateful to the National Natural Science Foundation of China (Grant Nos. 61275035, 61370046, and 51475200), Chinese National Programs for High Technology Research and Development (863 program:2013AA030902), the Key Technology Research and Development Program of Changchun (Grant No. 13KG66), Guangdong Natural Science Funds for Distinguished Young Scholar (Grant No. 2014A030306005), Scientific Frontier and Interdiscipline Innovative Projects of Jilin University (Grant No. 2013ZY18), and the Graduate Innovation Fund of Jilin University (Grant No. 2014021).

■ REFERENCES

(1) Chang, C. Y.; Zuo, L.; Yip, H. L.; Li, C. Z.; Li, Y.; Hsu, C. S.; Cheng, Y. J.; Chen, H.; Jen, A. K. Y. Highly Efficient Polymer Tandem Cells and Semitransparent Cells for Solar Energy. *Adv. Energy Mater.* **2013**, *4*, 1−6.

(2) Guo, F.; Ameri, T.; Forberich, K.; Brabec, C. J. Semitransparent Polymer Solar Cells. *Polym. Int.* **2013**, *62*, 1408−1412.

(3) Chueh, C. C.; Chien, S. C.; Yip, H. L.; Salinas, J. F.; Li, C. Z.; Chen, K. S.; Chen, F. C.; Chen, W. C.; Jen, A. K. Y. Toward High-Performance Semi-Transparent Polymer Solar Cells: Optimization of Ultra-Thin Light Absorbing Layer and Transparent Cathode Architecture. *Adv. Energy Mater.* **2013**, *3*, 417−423.

(4) Chen, K.-S.; Salinas, J.-F.; Yip, H.-L.; Huo, L.; Hou, J.; Jen, A. K. Y. Semitransparent Polymer Solar Cells with 6% PCE, 25% Average Visible Transmittance and a Color Rendering Index Close to 100 for Power Generating Window Applications. *Energy Environ. Sci.* **2012**, *5*, 9551−9557.

(5) Chang, C.-Y.; Zuo, L.; Yip, H.-L.; Li, Y.; Li, C.-Z.; Hsu, C.-S.; Cheng, Y.-J.; Chen, H.; Jen, A. K. Y. A Versatile Fluoro-Containing Low-Bandgap Polymer for Efficient Semitransparent and Tandem Polymer Solar Cells. *Adv. Funct. Mater.* **2013**, *23*, 5084−5090.

(6) Guo, F.; Kubis, P.; Stubhan, T.; Li, N.; Baran, D.; Przybilla, T.; Spiecker, E.; Forberich, K.; Brabec, C. J. Fully Solution-Processing Route toward Highly Transparent Polymer Solar Cells. *ACS Appl. Mater. Interfaces* **2014**, *6*, 18251−18257.

(7) Lee, K.-T.; Lee, J. Y.; Seo, S.; Guo, L. J. Colored Ultrathin Hybrid Photovoltaics with High Quantum Efficiency. *Light: Sci. Appl.* **2014**, *3*, No. e215.

(8) Meiss, J.; Leo, K.; Riede, M. K.; Uhrich, C.; Gnehr, W.-M.; Sonntag, S.; Pfeiffer, M. Efficient Semitransparent Small-Molecule Organic Solar Cells. *Appl. Phys. Lett.* **2009**, *95*, No. 213306.

(9) Yoon, J.; Baca, A. J.; Park, S.-I.; Elvikis, P.; Geddes, J. B.; Li, L.; Kim, R. H.; Xiao, J.; Wang, S.; Kim, T.-H. Ultrathin Silicon Solar Microcells for Semitransparent, Mechanically Flexible and Micro-concentrator Module Designs. *Nat. Mater.* **2008**, *7*, 907−915.

(10) Guo, F.; Zhu, X.; Forberich, K.; Krantz, J.; Stubhan, T.; Salinas, M.; Halik, M.; Spallek, S.; Butz, B.; Spiecker, E. ITO-free and Fully Solution-Processed Semitransparent Organic Solar Cells with High Fill Factors. *Adv. Energy Mater.* **2013**, *3*, 1062−1067.

(11) Krantz, J.; Stubhan, T.; Richter, M.; Spallek, S.; Litzov, I.; Matt, G. J.; Spiecker, E.; Brabec, C. J. Spray-Coated Silver Nanowires as Top Electrode Layer in Semitransparent P3HT:PCBM-Based Organic Solar Cell Devices. *Adv. Funct. Mater.* **2013**, *23*, 1711−1717.

(12) Zhang, D.-D.; Jiang, X.-C.; Wang, R.; Xie, H.-J.; Ma, G.-F.; Ou, Q.-D.; Chen, Y.-L.; Li, Y.-Q.; Tang, J.-X. Enhanced Performance of Semitransparent Inverted Organic Photovoltaic Devices via a High Reflector Structure. *ACS Appl. Mater. Interfaces* **2013**, *5*, 10185−10190.

(13) Park, B.; Yun, S. H.; Cho, C. Y.; Kim, Y. C.; Shin, J. C.; Jeon, H. G.; Huh, Y. H.; Hwang, I.; Baik, K. Y.; Lee, Y. I.; Uhm, H. S.; Cho, G. S.; Choi, E. H. Surface Plasmon Excitation in Semitransparent Inverted Polymer Photovoltaic Devices and Their Applications as Label-Free Optical Sensors. *Light: Sci. Appl.* **2014**, *3*, No. e222.

(14) Chen, C.-C.; Dou, L.; Zhu, R.; Chung, C.-H.; Song, T.-B.; Zheng, Y. B.; Hawks, S.; Li, G.; Weiss, P. S.; Yang, Y. Visibly Transparent Polymer Solar Cells Produced by Solution Processing. *ACS Nano* **2012**, *6*, 7185−7190.

(15) Beiley, Z. M.; Christoforo, M. G.; Gratia, P.; Bowring, A. R.; Eberspacher, P.; Margulis, G. Y.; Cabanetos, C.; Beaujuge, P. M.; Salleo, A.; McGehee, M. D. Semi-transparent Polymer Solar Cells with Excellent Sub-Bandgap Transmissionfor Third Generation Photovoltaics. *Adv. Mater.* **2013**, *25*, 7020−7026.

(16) Tang, Z.; George, Z.; Ma, Z.; Bergqvist, J.; Tvingstedt, K.; Vandewal, K.; Wang, E.; Andersson, L. M.; Andersson, M. R.; Zhang, F. Semi-transparent Tandem Organic Solar Cells with 90% Internal Quantum Efficiency. *Adv. Energy Mater.* **2012**, *2*, 1467−1476.

(17) Lin, H.-W.; Chen, Y.-H.; Huang, Z.-Y.; Chen, C.-W.; Lin, L.-Y.; Lin, F.; Wong, K.-T. Highly Efficient Bifacial Transparent Organic Solar Cells with Power Conversion Efficiency Greater than 3% and Transparency of 50%. *Org. Electron.* **2012**, *13*, 1722−1728.

(18) Yu, W. J.; Shen, L.; Long, Y. B.; Shen, P.; Guo, W. B.; Chen, W. Y.; Ruan, S. P. Highly Efficient and High Transmittance Semi-transparent Polymer Solar Cells with One-Dimensional Photonic Crystals as Distributed Bragg Reflectors. *Org. Electron.* **2014**, *15*, 470−477.

(19) Colsmann, A.; Reinhard, M.; Kwon, T.-H.; Kayser, C.; Nickel, F.; Czolk, J.; Lemmer, U.; Clark, N.; Jasieniak, J.; Holmes, A. B.; Jones, D. Inverted Semi-Transparent Organic Solar Cells with Spray Coated, Surfactant Free Polymer Top-Electrodes. *Sol. Energy Mater. Sol. Cells* **2012**, *98*, 118−123.

(20) Kim, H. P.; Lee, H. J.; Yusoff, A. R. b. M.; Jang, J. Semi-transparent Organic Inverted Photovoltaic Cells with Solution Processed Top Electrode. *Sol. Energy Mater. Sol. Cells* **2013**, *108*, 38−43.

(21) Zhou, Y.; Cheun, H.; Choi, S.; Fuentes-Hernandez, C.; Kippelen, B. Optimization of a Polymer Top Electrode for Inverted Semitransparent Organic Solar Cells. *Org. Electron.* **2011**, *12*, 827−831.

(22) Ameri, T.; Dennler, G.; Waldauf, C.; Azimi, H.; Seemann, A.; Forberich, K.; Hauch, J.; Scharber, M.; Hingerl, K.; Brabec, C. J. Fabrication, Optical Modeling, and Color Characterization of

DOI: 10.1021/acsami.5b02039
ACS Appl. Mater. Interfaces 2015, 7, 9920−9928

Semitransparent Bulk-Heterojunction Organic Solar Cells in an Inverted Structure. *Adv. Funct. Mater.* **2010**, *20*, 1592−1598.
(23) Li, X. F.; Budai, J. D.; Liu, F.; Howe, J. Y.; Zhang, J. H.; Wang, X. J.; Gu, Z. J.; Sun, C. J.; Meltzer, R. S.; Pan, Z. W. New Yellow $Ba_{0.93}Eu_{0.07}Al_2O_4$ Phosphor for Warm-White Light-Emitting Diodes Through Single-Emitting-Center Conversion. *Light: Sci. Appl.* **2013**, *2*, No. e50.
(24) Chen, C.-C.; Dou, L.; Gao, J.; Chang, W.-H.; Li, G.; Yang, Y. High-Performance Semi-transparent Polymer Solar Cells Possessing Tandem Structures. *Energy Environ. Sci.* **2013**, *6*, 2714−2720.
(25) Mescher, J.; Kettlitz, S. W.; Christ, N.; Klein, M. F.; Puetz, A.; Mertens, A.; Colsmann, A.; Lemmer, U. Design Rules for Semi-transparent Organic Tandem Solar Cells for Window Integration. *Org. Electron.* **2014**, *15*, 1476−1480.
(26) Czolk, J.; Puetz, A.; Kutsarov, D.; Reinhard, M.; Lemmer, U.; Colsmann, A. Inverted Semi-transparent Polymer Solar Cells with Transparency Color Rendering Indices Approaching 100. *Adv. Energy Mater.* **2013**, *3*, 386−390.
(27) Colsmann, A.; Puetz, A.; Bauer, A.; Hanisch, J.; Ahlswede, E.; Lemmer, U. Efficient Semi-transparent Organic Solar Cells with Good Transparency Color Perception and Rendering Properties. *Adv. Energy Mater.* **2011**, *1*, 599−603.
(28) Xiang, C.; Koo, W.; So, F.; Sasabe, H.; Kido, J. A Systematic Study on Efficiency Enhancements in Phosphorescent Green, Red and Blue Microcavity Organic Light Emitting Devices. *Light: Sci. Appl.* **2013**, *2*, No. e74.
(29) Commission Internationale de ÍÉclairage International 1995, ISBN 3-900-734-57-7.
(30) *CIE Standard Illuminants for Colorimetry*, ISO 10526:1999/CIE S005/E-1998; International Organization for Standardization (ISO): Geneva, Switzerland, 1999.
(31) Blouin, N.; Michaud, A.; Leclerc, M. A Low-Bandgap Poly (2, 7-Carbazole) Derivative for Use in High-Performance Solar Cells. *Adv. Mater.* **2007**, *19*, 2295−2300.
(32) Zilberberg, K.; Behrendt, A.; Kraft, M.; Scherf, U.; Riedl, T. Ultrathin Interlayers of a Conjugated Polyelectrolyte for Low Work-Function Cathodes in Efficient Inverted Organic Solar Cells. *Org. Electron.* **2013**, *14*, 951−957.
(33) Park, S. H.; Roy, A.; Beaupre, S.; Cho, S.; Coates, N.; Moon, J. S.; Moses, D.; Leclerc, M.; Lee, K.; Heeger, A. J. Bulk Heterojunction Solar Cells with Internal Quantum Efficiency Approaching 100%. *Nat. Photonics* **2009**, *3*, 297−302.
(34) Betancur, R.; Romero-Gomez, P.; Martinez-Otero, A.; Elias, X.; Maymo, M.; Martorell, J. Transparent Polymer Solar Cells Employing a Layered Light-Trapping Architecture. *Nat. Photonics* **2013**, *7*, 995−1000.
(35) Yu, W.; Shen, L.; Shen, P.; Long, Y.; Sun, H.; Chen, W.; Ruan, S. Semitransparent Polymer Solar Cells with 5% Power Conversion Efficiency Using Photonic Crystal Reflector. *ACS Appl. Mater. Interfaces* **2014**, *6*, 599−605.
(36) Yu, W.; Shen, L.; Long, Y.; Guo, W.; Meng, F.; Ruan, S.; Jia, X.; Ma, H.; Chen, W. Semitransparent Polymer Solar Cells with One-Dimensional $(WO_3/LiF)(N)$ Photonic Crystals. *Appl. Phys. Lett.* **2012**, *101*, No. 153307.
(37) Joannopoulos, J. D.; Villeneuve, P. R.; Fan, S. Photonic Crystals: Putting a New Twist on Light. *Nature* **1997**, *386*, 143−149.
(38) Winn, J. N.; Fink, Y.; Fan, S.; Joannopoulos, J. Omnidirectional Reflection from a One-Dimensional Photonic Crystal. *Opt. Lett.* **1998**, *23*, 1573−1575.
(39) Bendickson, J. M.; Dowling, J. P.; Scalora, M. Analytic Expressions for the Electromagnetic Mode Density in Finite, One-Dimensional, Photonic Band-Gap Structures. *Phys. Rev. E* **1996**, *53*, 4107−4121.
(40) Talghader, J. J.; Gawarikar, A. S.; Shea, R. P. Spectral Selectivity in Infrared Thermal Detection. *Light: Sci. Appl.* **2012**, *1*, No. e24.
(41) Dardano, P.; Gagliardi, M.; Rendina, I.; Cabrini, S.; Mocella, V. Ellipsometric Determination of Permittivity in a Negative Index Photonic Crystal Metamaterial. *Light: Sci. Appl.* **2012**, *1*, No. e42.
(42) Enrich, R. M.; Llobera, A.; Planas, J. V.; Cadarso, V. J.; Mompart, J.; Ahufinger, V. Light Spectral Filtering Based on Spatial Adiabatic Passage. *Light: Sci. Appl.* **2013**, *2*, No. e90.
(43) Fröbel, M.; Schwab, T.; Kliem, M.; Hofmann, S.; Leo, K.; Gather, M. C. Get It White: Color-Tunable AC/DC OLEDs. *Light: Sci. Appl.* **2015**, *4*, No. e247.
(44) Oh, J. H.; Yang, S. J.; Do, Y. R. Healthy, Natural, Efficient and Tunable Lighting: Four-Package White LEDs for Optimizing the Circadian Effect, Color Quality and Vision Performance. *Light: Sci. Appl.* **2014**, *3*, No. e141.
(45) Wyszecki, G.; Stiles, W. S. *Color Science: Concepts and Methods, Quantitative Data and Formulae*, 2nd ed.; Wiley-Interscience: New York, 2000; ISBN 0-471-39918-3.
(46) Borbély, Á.; Sámson, Á.; Schanda, J. The Concept of Correlated Colour Temperature Revisited. *Color Res. Appl.* **2001**, *26*, 450−457.
(47) Schanda, J. *Colorimetry: Understanding the CIE System*; John Wiley & Sons: Hoboken, NJ, USA, 2007; pp 71−73.
(48) Geusebroek, J.-M.; van den Boomgaard, R.; Smeulders, A. W.; Gevers, T. Color Constancy from Physical Principles. *Pattern Recognit. Lett.* **2003**, *24*, 1653−1662.
(49) Nickerson, D. Light Sources and Color Rendering. *J. Opt. Soc. Am.* **1960**, *50*, 57−68.
(50) Sergeant, N. P.; Hadipour, A.; Niesen, B.; Cheyns, D.; Heremans, P.; Peumans, P.; Rand, B. P. Design of Transparent Anodes for Resonant Cavity Enhanced Light Harvesting in Organic Solar Cells. *Adv. Mater.* **2012**, *24*, 728−732.
(51) Pettersson, L. A.; Roman, L. S.; Inganas, O. Modeling Photocurrent Action Spectra of Photovoltaic Devices Based on Organic Thin Films. *J. Appl. Phys.* **1999**, *86*, 487−496.
(52) Liu, Y. K.; Wang, S. C.; Li, Y. Y.; Song, L. Y.; Xie, X. S.; Feng, M. N.; Xiao, Z. M.; Deng, S. Z.; Zhou, J. Y.; Li, J. T.; Wong, K. S.; Krauss, T. F. Efficient Color Routing with a Dispersion-Controlled Waveguide Array. *Light: Sci. Appl.* **2013**, *2*, No. e52.
(53) Long, Y. Effects of Metal Electrode Reflection and Layer Thicknesses on the Performance of Inverted Organic Solar Cells. *Sol. Energy Mater. Sol. Cells* **2010**, *94*, 744−749.
(54) Eerenstein, W.; Slooff, L.; Veenstra, S.; Kroon, J. Optical Modeling as Optimization Tool for Single and Double Junction Polymer Solar Cells. *Thin Solid Films* **2008**, *516*, 7188−7192.

DOI: 10.1021/acsami.5b02039
ACS Appl. Mater. Interfaces 2015, 7, 9920−9928